# An experimental and theoretical study of the valence shell photoelectron spectrum of oxalyl chloride

D. M. P. Holland[a,*], S. Nandi[b,c], C. Nicolas[b], J. D. Bozek[b], M. Patanen[d], I. Powis[e]

[a] Daresbury Laboratory, Daresbury, Warrington, Cheshire WA4 4AD, UK

[b] Synchrotron SOLEIL, L'Orme des Merisiers, Saint-Aubin, BP 48, 91192 Gif-sur-Yvette, France

[c] Current address : Université de Lyon, Université Claude Bernard Lyon 1, CNRS, Institut Lumière Matière, F-69622, Villeurbanne, France

[d] Nano and Molecular Systems Research Unit, Faculty of Science, University of Oulu, P. O. Box 3000, 90014 Oulu, Finland

[e] School of Chemistry, University of Nottingham, Nottingham NG7 2RD, UK

[*] Corresponding author
*E-mail address:* david.holland@stfc.ac.uk

**Abstract**

Polarization dependent photoelectron spectra encompassing the outer valence orbitals of oxalyl chloride have been recorded in the photon energy range 19 – 91 eV. These have allowed photoelectron anisotropy parameters and branching ratios to be determined. Photoionization partial cross sections and photoelectron anisotropy parameters have been calculated with the Continuum Multiple Scattering – Xα approach. Four of the outer valence orbitals are predicted to possess a significant Cl 3*p* lone-pair character and have closely grouped binding energies. The photoionization dynamics of these four orbitals are predicted to be strongly affected by the Cooper minimum associated with the Cl 3*p* orbital in the isolated atom at photon energies around 40 eV. A comparison between the theoretical and measured photoelectron anisotropy parameters has enabled the molecular orbital sequence to be clarified. A doublet has been observed in the region of the photoelectron spectrum where a band due to the $5b_u$ orbital might be anticipated. Our calculations indicate that the $6b_u$ and $5b_u$ orbitals are coupled. This coupling may account for the apparent lack of a pronounced Cooper minimum in the $\beta$-parameter associated with the nominal $6b_u$ ionization and for the unexpected appearance of the adjacent photoelectron band, nominally associated with the $5b_u$ orbital. The vertical ionization energy of the outermost $7a_g$ orbital was experimentally determined to be 11.266±0.005 eV.

Keywords

Oxalyl chloride; Photoelectron angular distributions; Vibronic coupling; Cooper minima; Vibrational structure.

## 1. Introduction

The geometric structure of oxalyl chloride ($C_2Cl_2O_2$), a chlorine-substituted glyoxal, has long been, and continues to be, of considerable interest. An early electron diffraction and theoretical investigation [1] indicated that, in the gas phase, oxalyl chloride is a mixture of the *trans* and *gauche* conformers, with the *trans*-planar geometry ($C_{2h}$ symmetry) being the more stable. Torsion about the central C-C bond will rotate the *trans* conformer into *gauche* and then *cis* geometries. Subsequent experimental evidence confirmed the presence, in the gas phase, of the second conformer (*gauche*), but the theoretical verification of this prediction showed a strong dependence on the level of calculation and the employed basis sets [2-5]. A recent investigation, in which all three conformers were studied theoretically, confirmed the existence of the *trans* and *gauche* conformers in the gas phase [6].

Far less attention has been focussed on the electronic structure of oxalyl chloride. Experimental investigations of the spectroscopic and photochemical properties include photoelectron spectroscopy [7,8], photolysis [9] and photodissociation [6,10]. In the photoionization experiment performed by Chu et al [6], parent and fragment ion yields were measured using synchrotron radiation. These authors estimated that, in the gas phase, the main conformers are *trans* (~70%) and *gauche* (~30%), with very little *cis* conformer. An observed second onset in the parent ion yield was attributed to the *cis* conformer, formed through conformational conversion after ionization [6]. In the present work, only the *trans* conformer will be considered in detail.

The photoelectron spectrum of oxalyl chloride [7,8], recorded with HeI radiation, exhibits predominantly broad bands, with weak vibrational structure evident in the binding energy range ~14.8 – 15.9 eV. Photoelectron angular distributions, which often provide additional information that can help correlate the observed bands with ionization from specific orbitals, have previously not been determined. Such measurements may be particularly useful in congested regions of the photoelectron spectrum where adjacent orbitals with similar binding energies overlap one another.

The valence shell molecular orbital sequence of oxalyl chloride, in its neutral ground state and assuming $C_{2h}$ symmetry, may be given as:

$(1a_g)^2\ (1b_u)^2\ (2a_g)^2\ (2b_u)^2\ (3a_g)^2\ (3b_u)^2\ (4a_g)^2\ (4b_u)^2\ (5a_g)^2\ (1a_u)^2\ (1b_g)^2\ (5b_u)^2\ (6b_u)^2\ (2b_g)^2\ (2a_u)^2\ (6a_g)^2\ (7a_g)^2 \quad \tilde{X}\ ^1A_g$

where the numbering of the molecular orbitals ignores the atomic-like core orbitals. As will be discussed, however, we find the calculation of orbital ordering does depend on the model chemistry employed, which may explain some discrepancies in the earlier literature [7,8]. Mulliken population analyses [11] (see Table S1, Supplementary material) clearly indicate that many of the outer valence orbitals of oxalyl chloride may be considered as possessing a dominant localised atomic character.

In a series of experimental and theoretical investigations [12-17], we have studied the manner in which the dominant atomic character of a molecular orbital influences the photoionization dynamics. Specifically, photoionization partial cross sections ($\sigma$) and photoelectron angular distributions, characterised by the anisotropy parameter ($\beta$), have been measured in several chlorine-containing molecules, and the experimental results have been compared to the corresponding theoretical results calculated with the Continuum Multiple Scattering (CMS)-Xα approach [12,18]. The comparison shows that for molecular orbitals having a significant Cl 3*p* content the photoionization partial cross sections and photoelectron anisotropy parameters display energy dependent variations which resemble those predicted for ionization of atomic Cl 3*p* [19]. In an atom, the Cooper minimum [20,21] associated with the Cl 3*p* orbital [19] results in a fairly isotropic photoelectron angular distribution ($\beta \sim 0$) and in a reduction in the partial cross section in the photon energy range around 40 eV. Such effects can be used to assess the extent to which a molecular orbital having a predominantly atomic character is modified by the molecular environment. Moreover, the energy dependent variations can help identify an essentially atomic-like molecular orbital even in congested regions of the photoelectron spectrum where individual photoelectron bands overlap.

In the present work, polarization dependent photoelectron spectra encompassing the bands due to ionization of the outer valence orbitals of oxalyl chloride have been recorded, using plane polarized synchrotron radiation, in the photon energy range 19 – 91 eV. These have allowed electronic state intensity branching ratios (related to the photoionization partial cross sections) and photoelectron anisotropy parameters to be determined. The CMS-Xα method has been employed to calculate the corresponding theoretical values. In addition, the vibrational structure observed in the photoelectron band associated with the $1b_g$ orbital has been assigned through comparison with the vibrational energies for the neutral $\tilde{X}\,^1A_g$ state [3].

## 2. Experimental apparatus and procedure

The experiments were carried out on the soft X-ray undulator-based PLÉIADES beamline at the SOLEIL synchrotron radiation facility. Detailed descriptions of the beamline and station instrumentation have been reported previously [22], so only a summary is given here.

Plane polarized synchrotron radiation (>99% [23]), derived from an Apple II type undulator, was monochromated with a plane grating, modified-Petersen type monochromator and delivered into the interaction region of a VG Scienta R4000 electron analyser. The plane of linear polarization could be rotated through 90°, thereby allowing photoelectron angular distributions to be measured with the electron analyser in a fixed position.

The photoelectron spectra encompassing the bands due to ionization of the outer valence orbitals were recorded with a monochromator slit width of 50 μm, using a 400 lines/mm grating. At photon energies of 19 and 91 eV, this corresponds to theoretical optical resolutions of ~1 and 7 meV, respectively. The complete valence shell photoelectron spectrum, measured at a photon energy of 80 eV, used a 600 lines/mm grating and an exit slit width of 125 μm, resulting in a theoretical optical resolution of 25 meV.

The outer valence shell photoelectron spectra were recorded with an analyser pass energy of 10 eV and a 0.3 mm curved entrance slit width, resulting in a theoretical spectrometer

resolution of 7.5 meV. The complete valence shell photoelectron spectrum was recorded with the same pass energy but with a 0.2 mm curved entrance slit width, giving a theoretical spectrometer resolution of 5 meV.

Translational Doppler broadening, associated with the thermal motion of the room temperature sample molecules, contributes to the photoelectron peak width [24]. For example, at a photon energy of 40 eV, this broadening amounts to ~6 meV for the peak due to the $\tilde{X}\,^2A_g$ state.

Taking the convolution of the optical and electron energy resolutions, and the Doppler broadening, suggests an overall resolution of ~10 meV was achieved for the outer valence region spectra.

Photoelectron spectra were recorded with the plane of polarization set either parallel ($\theta$ = 0º) or perpendicular ($\theta$ = 90º) to the direction of the electron's path towards the detector. Assuming electric dipole photoionization by completely plane polarized radiation, the differential photoionization partial cross section can be expressed as [25]

$$\frac{\mathrm{d}\sigma}{\mathrm{d}\Omega} = \frac{\sigma}{4\pi}\left[1+\beta\,\mathrm{P}_2\left(\cos\theta\right)\right] \qquad (1)$$

where $\sigma$ is the angle-integrated partial cross section, dΩ is the differential solid angle element in the direction specified by the polar angle $\theta$, $\beta$ is the photoelectron anisotropy parameter, $P_2(\cos\theta)$ is the Legendre polynomial of second order, and $\theta$ is the electron ejection angle relative to the plane of polarization. Eq (1) can be rearranged into the more convenient form [22]

$$\beta = \frac{2\left(I_0 - I_{90}\right)}{I_0 + 2I_{90}} \qquad (2)$$

where $I_0$ and $I_{90}$ are the normalized electron intensities for parallel and perpendicular polarization orientations relative to the electron detection axis, respectively. All the spectra

were normalized to the sample pressure, the accumulation time, and the photon flux prior to processing. The transmission efficiency of the electron analyser was determined, as described by Jauhiainen et al [26], and all the spectra were corrected for this variation.

The experimental photoelectron anisotropy parameter and branching ratio associated with a particular binding energy range were determined as described by Powis et al [22]. Table 1 lists the binding energy ranges used to analyse the photoelectron spectra of oxalyl chloride. Within each range, a mean $\beta$-parameter is evaluated by summing the electron counts in the normalized parallel and perpendicular polarization dependent spectra and inserting these summed intensities into Eq (2). The intensities required for the branching ratios are evaluated in a similar manner. These mean $\beta$-parameters and branching ratios are thus vibrationally averaged values. In our discussion of the experimental results, such $\beta$-parameters and branching ratios are compared with the corresponding theoretical predictions obtained in a fixed nuclei calculation. Our analysis procedure also allows the variation in the $\beta$-parameter as a function of the binding energy across a specific photoelectron band to be determined, thereby enabling the variation in the $\beta$-value associated with specific vibrational excitations to be observed. This capability has been employed to study the variation in the $\beta$-parameter, corresponding to the excitation of particular vibrational modes, in the $(1b_g)^{-1}$ state photoelectron band.

Some of the spectra shown in this paper are so-called magic angle spectra ($\theta$ = 54.7º), where the electron intensity is independent of the photoelectron anisotropy parameter. Such magic angle spectra are synthesised from the spectra measured at $\theta$ = 0º and $\theta$ = 90º using the expression [23]

$$I_{54.7} = \frac{I_0 + 2I_{90}}{3} \qquad (3)$$

Oxalyl chloride is a liquid with a significant vapour pressure (~150 mmHg) at room temperature (~20 ºC). After several freeze-pump-thaw cycles, the sample vapour was admitted, without any further heating, into a gas cell in the experimental chamber.

Despite attempts to remove volatile impurities, the valence shell photoelectron spectra of oxalyl chloride always exhibited some weak, superimposed sharp peaks that could be attributed to HCl, CO and $CO_2$. Fig. S1 in Supplementary material shows an expanded spectrum with all peaks due to impurities identified. This impurity signal persisted, without reduction, throughout the entire beamtime. The electron binding energy scale was calibrated using the well-established ionization energies of the outer valence ionic states of CO [27] and $CO_2$ [28,29].

## 3. Computational details

Calculations to identify and order the molecular orbitals for the optimised $C_{2h}$ *trans*-planar geometry of oxalyl chloride were compared for a variety of model chemistries using Gaussian 16 software [30]; this included Møller-Plesset (MP2) and density functional theory (DFT) methods employing B3LYP and Xα functionals, and basis sets ranging from double- to quadruple-$\zeta$ quality were evaluated. Ionization energies were estimated by the outer valence Green's function (OVGF) method [31,32] and by the equation of motion coupled cluster method for ionization potentials (EOM-IP-CCSD), the latter as implemented in Q-Chem [33-35]. Further estimates of the cation electronic state excitation energies were obtained using TD-DFT - B3LYP calculations that were made using both Gaussian 16 and Q-Chem.

The OVGF and EOM-IP-CCSD calculations were also repeated to estimate vertical ionization energies at the equilibrium geometry of the *gauche* conformer.

Photoionization cross sections, hence electronic branching ratios, and photoelectron anisotropy parameters were calculated by the CMS-Xα method which we have previously described [12,18]. A brief summary can be given as follows. Starting from atomic coordinates derived from a MP2/6-311G** geometry optimization, a model potential was constructed by overlapping spherical regions, with radii given by a Norman procedure, scaled by a factor 0.88 and situated on each atomic centre and fully enclosed within an outer spherical region. Within this framework, the exchange contribution to an effective one-

electron potential is represented using the Xα local density approximation. Self-consistent solutions are obtained from the initial trial guess using a symmetry adapted basis of spherical harmonic functions in each region. For the neutral ground state, these expansions were truncated at $l_{max}$ values of 7;3;2;2 for, respectively, the outer sphere, chlorine, oxygen and carbon regions. For the final state, the iterated potential is adapted to have the correct Coulombic form expected for ion plus electron in the asymptotic region, and the basis set expansion increased to $l_{max}$= 10;6;5;5. Maintaining an orthogonal set of bound orbitals for neutral and cation, photoionization matrix elements are then calculated in a one-electron formulation, and thence cross sections and anisotropy parameters obtained. Systematic checks were made to assure for adequate convergence of the calculated photoionization matrix elements.

## 4. Results and discussion

### *4.1. Overview of the valence shell photoelectron spectrum*

Our MP2 calculations with basis sets of at least triple-$\zeta$ quality (cc-pVTZ, cc-PVQZ, 6-311G**) provide a consistent identification and ordering for the molecular orbitals of *trans*-oxalyl chloride ($C_{2h}$), as indicated in the Introduction and Table 2. However, MP2 calculations made with a smaller double-$\zeta$ basis (6-31G*) return a reversed ordering for the $6a_g$ and $2a_u$ pair. Alternative computational approaches using DFT methods can be summarised as follows. Those calculations using B3LYP exchange-correlation functional all switch the ordering of the $2b_g/6b_u$ pair *and* the $1a_u/5a_g$ pair in comparison to the MP2 calculations with the same basis sets, except again for the B3LYP/6-31G* calculation which exchanges just the $6a_g/2a_u$ pair. Similar orbital switching patterns occur using the Xα exchange functional, although it is pertinent to note that the MS-Xα calculation used in the later calculation of photoionization dynamics switches only the $2b_g/6b_u$ order compared to the MP2 reference calculations.

Iso-surface plots illustrating the symmetry and characteristics of the eight highest occupied orbitals in the ground state neutral molecule (ordered as our preferred MP2/triple-$\zeta$ calculations) are shown in Fig. 1. These visual representations and populations allow the

character of a molecular orbital to be assessed, complementing the numerical Mulliken atomic populations [11] listed in Table S1, Supplementary material. The outermost orbital, $7a_g$, has a mixed oxygen lone-pair and chlorine lone-pair character. The next four orbitals ($6a_g$, $2a_u$, $2b_g$, $6b_u$) are composed of various combinations of the Cl 3*p* lone-pairs. Two of these orbitals ($6a_g$ and $6b_u$) comprise essentially in-plane chlorine lone-pairs, while the other two ($2a_u$ and $2b_g$) comprise mainly out-of-plane chlorine lone-pairs together with a smaller contribution from the out-of-plane O 2*p* lone-pairs. For brevity, we will henceforth use σ or π to identify, respectively, the in-plane or out-of-plane orientation of the Cl 3*p* or O 2*p* orbitals. The $5b_u$ orbital may be characterised as mainly an in-plane O 2*p* lone-pair, whilst the $1b_g$ and $1a_u$ orbitals correspond to π-bonding between the C and O atoms.

Fig. 2 shows a magic angle photoelectron spectrum obtained at a photon energy of 19 eV. At this excitation energy, apart from extremely weak features due to the $HCl^+$ $X\ ^2\Pi_{3/2,1/2}$ $v^+ = 0$ states at 12.745 and 12.827 eV [36], and the $CO^+$ $X\ ^2\Sigma$ $v^+ = 0$ state at 14.014 eV [27], all the observed structure is believed to be associated with ionization of oxalyl chloride.

Although a first step to assigning the photoelectron bands would often be a direct mapping of the calculated orbital ordering and spacing using Koopmans' theorem, this is clearly problematic here. Table 2 lists the Koopmans' ionization energies (negative canonical orbital energy) obtained from the MP2/cc-pVQZ calculation. The rms deviation of the MP2 orbital energies obtained with the cc-pVDZ or cc-pVTZ bases is just 0.055 eV, increasing to 0.099 eV for the 6-311G** basis, but it is immediately evident that the MP2 Koopmans' energies are consistently more than 1 eV too high compared to the experimental spectrum (Fig. 2). (The magnitude of B3LYP Kohn-Sham orbital energies are an even worse guide to the experimental ionization energies.)

More reliable estimates of the vertical ionization energies from the ground state equilibrium geometry are obtained using methods offering better treatments of electron correlation. The outer valence Green's function (OVGF) method uses electron propagator techniques, and assuming an independent particle picture of ionization holds [37], provides vertical ionization

energies that are typically expected to be within 0.3 eV of experimental values [31]. Table 2 includes OVGF ionization energies calculated using aug-cc-pVTZ and cc-pVQZ basis sets. Alternative results using the Equation of Motion Coupled Cluster method for Ionization Potentials (EOM-IP-CCSD) [34] also appear in Table 2. This approach is generally found to be highly accurate for the calculation of excitation energies, typically achieving accuracies better than 0.3 eV. Both of these correlated methods reverse the Koopmans' approximation ordering of the $1a_u/5a_g$ orbital pair. The vertical ionization energies obtained by the EOM-IP-CCSD method are marked in Fig. 2 and seem to offer a satisfactory overall interpretation of the experimental spectrum up to a binding energy of ~16 eV.

Complementing these methods, the vertical excitation energies of the excited ionic states were computed using TD-DFT calculations with a B3LYP functional. To facilitate comparisons, these electronic excitations (relative to the ground $7a_g^{-1}$ *ion* state, but evaluated at the ground state *neutral* geometry) are expressed as estimated vertical ionization energies by adding an assumed $I_{vert}$ (11.4 eV) for the ground state ion. Example results obtained in this manner complete Table 2.

While the preceding discussion has been focussed on the lowest energy *trans* ($C_{2h}$) oxalyl chloride, we briefly now consider other conformers. The torsional potential for variation in the Cl-C-C-Cl dihedral angle, identifying the torsional conformers (*cis*, *trans*, *gauche*) is shown in Fig. S2 in Supplementary material. As summarised in Ref. [6], the existence of these three structures has been a topic of experimental and theoretical interest, but the most energetic, unstable *cis* conformer can be rather immediately discounted for having a negligible population at room temperature. The *gauche* form, on the other hand, has a calculated excitation energy of ~0.002 a.u. according to the B3LYP/cc-pVDZ results in Fig. S2, leading to a predicted population of ~10% at 300K. More accurate CCSD/aug-cc-pVTZ calculations made here return a reduced absolute energy separation of 0.0013 a.u., corresponding to a 300K Boltzmann population of ~20%. While not themselves definitive calculations, these results broadly accord with an earlier population estimate of 30%, made by applying basis set corrections and with allowance for internal vibrational excitations [6]. It

may be noted that the potential around the gauche conformer at 90$^{o}$ is very flat (Fig. S2), and at 300K large amplitude torsional motions can be anticipated to complicate a full theoretical assessment.

Vertical ionization energies calculated at the *gauche* equilibrium geometry are included for comparison in Fig. 2. Due to the lowered symmetry ($C_1$) these are not labelled by irreducible representation. Above 13 eV they increasingly diverge from the *trans* ionization predictions. Moreover, these *gauche* energies are then not so clearly correlated with any experimental structure, and do not appear to offer any additional insight into possible assignments. Henceforward, we discuss the spectra solely in terms of the majority *trans* conformer.

Experimentally, the outermost photoelectron band, with a maximum at a binding energy of 11.266 eV, undoubtedly arises from ionization of the $7a_g$ orbital (Fig. 2). According to our calculations, the next prominent band observed in the binding energy range ~12.0 – 13.3 eV is due to ionization of the $6a_g$, $2a_u$, $2b_g$ and $6b_u$ orbitals, with the individual contributions from these orbitals overlapping significantly. Shoulders are evident in the experimental spectrum at ~12.35 and 13.05 eV. Although the predicted energetic separations of these states are ~0.1 eV (Table 2), this ordering is given consistently by calculations beyond the simple Koopmans' approximation that incorporate some correction for correlation energy. There is, however, no treatment for possible spin-orbit interaction in these calculations. In the atomic limit, Cl 3*p* spin-orbit splittings, also of ~0.1 eV, might be expected, but experimentally there are no discernible indications of this for these nominally lone-pair molecular orbitals. More subtly, coupling with O lone-pairs ($2a_u$, $2b_g$) may be influenced, but again not at a currently resolvable level.

A doublet, which may be associated with the $5b_u$ orbital, appears around 13.5 eV (Fig. 2). Next, a complicated photoelectron band, exhibiting vibrational structure, occurs between ~14.7 and 16.0 eV, which our calculations consistently identify as ionization of the $1b_g$ orbital.

Several broad intense features are observed at higher binding energies. Before attempting assignments, one needs to acknowledge the presence of persistent impurity bands, particularly in this region. A complete valence shell photoelectron spectrum, recorded at a photon energy of 80 eV using parallel polarized radiation, is shown as an inset to Fig. 2. Most of the weak but sharp peaks appearing at binding energies below 20 eV are due to ionization of HCl, CO and $CO_2$ (see Fig. S1 in Supplementary material which clearly identifies and assigns all impurity peaks). Nevertheless, the overall contribution from impurities is small (the sharpness of the impurity peaks tends to emphasise their presence) and the broad peaks appearing in the spectrum at binding energies above 20 eV should not be strongly affected by impurities.

Returning to consider the 16 – 18 eV region, spectra recorded at photon energies above ~35 eV exhibit shoulders at 16.55, 16.75 and 16.93 eV (see section 4.3) that appear to be due to oxalyl chloride. The calculated ionization energy of the $5a_g$ orbital (~16.5 eV) closely matches that of the first shoulder, and the $1a_u$ orbital, with calculated ionization energies around 16.8 – 17.10 eV, appears to correlate with the third of these shoulders. In this region, above the $1b_g^{-1}$ state, the TD-DFT calculations identify several states involving excitations from the ground state cation into virtual orbitals, leaving two-hole, high spin states that in the single, independent electron model for direct ionization of the ground state neutral would be inaccessible. This, and the falling pole strengths of the OVGF calculations, may flag the incipient breakdown of the independent particle assumption above 16 eV.

### *4.2. Vibrational excitations associated with the $1b_g$ orbital*

Fig. 3 shows the photoelectron band due to ionization of the $1b_g$ orbital, recorded at a photon energy of 23 eV using parallel polarized radiation. The vibrational structure can be assigned to four progressions, each involving excitation of the $\nu_1^+(a_g)$ mode, either alone, or in combination with one or two quanta of the $\nu_5^+(a_g)$ mode, or one quanta of the $\nu_2^+(a_g)$ mode, as detailed in Table 3. Our spectra yield vibrational energies of 230, 140 and 40 meV for the $\nu_1^+$, $\nu_2^+$ and $\nu_5^+$ modes, respectively, based on the spacing between the peak due to the adiabatic transition and that associated with the first member in each progression. The

corresponding energies in the neutral ground state are 221.3, 133.9 and 33.8 meV, for the $\nu_1$, $\nu_2$ and $\nu_5$ modes, respectively [3].

### *4.3. Photoelectron angular distributions and branching ratios*

As already discussed, two of the molecular orbitals ($6a_g$ and $6b_u$) in oxalyl chloride may be characterised as almost pure σ-type Cl 3*p* lone-pairs, whilst the $2a_u$ and $2b_g$ orbitals possess a significant π-type Cl 3*p* lone-pair character together with a smaller contribution of π-type O 2*p* lone-pair character (Fig. 1). The outermost $7a_g$ orbital has a mixed σ-type Cl 3*p* and σ-type O 2*p* character. Thus, many of the molecular orbitals of oxalyl chloride possess a strong atomic *p*-type character.

The photoionization dynamics governing atomic *p*-type orbitals are well established [20,21]. Electric dipole selection rules restrict the orbital angular momentum ($l$) of a photoelectron ejected from an initial *p*-type orbital ($l = 1$) to $l - 1$ (a $p \rightarrow s$ transition) or $l + 1$ (a $p \rightarrow d$ transition). Theoretical studies have shown that the radial matrix element for the dominant $p \rightarrow d$ transition can change sign, provided that the initial wave function contains a node. At the energy coinciding with the change in sign of the $p \rightarrow d$ channel, only the $p \rightarrow s$ channel contributes amplitude to the photoionization partial cross section, which consequently exhibits a minimum (often referred to as a Cooper minimum). Often more strikingly, the photoelectron angular distribution becomes isotropic, corresponding to $\beta = 0$. In oxalyl chloride, the relevant orbitals are Cl 3*p* and O 2*p*. The Cl 3*p* orbital contains a node whereas the O 2*p* orbital does not [19]. In atomic photoionization, the $\beta$-parameter for the Cl 3*p* orbital passes through the Cooper minimum at an electron kinetic energy of ~30 eV, while the value of the $\beta$-parameter for the O 2*p* orbital increases steadily as the electron kinetic energy increases [19].

We begin the discussion of our results by considering whether the calculated photoelectron angular distributions ($\beta$-parameters) for specific molecular orbitals (Fig. 4) display an energy dependence typical of that predicted for a Cl 3*p* lone-pair, an O 2*p* lone-pair, or a π-orbital. The calculated $\beta$-parameters for the $6a_g$ and $6b_u$ orbitals, both of which are essentially in-

plane Cl 3*p* lone-pairs, become almost isotropic ($\beta$~0) around $h\nu \approx 40$ eV — very closely resembling the predicted behaviour and Cooper minimum obtained for an atomic Cl 3*p* orbital [19]. The calculated $\beta$-parameters for the $2a_u$ and $2b_g$ orbitals also exhibit a dip around 40 eV, but the dip is not as pronounced as that for the $6a_g$ and $6b_u$ orbitals. As the $2a_u$ and $2b_g$ orbitals contain some O 2*p* lone-pair character in addition to the stronger Cl 3*p* lone-pair contribution, the theoretical results for these two orbitals appear consistent with expectations based upon orbital characteristics.

The calculated $\beta$-parameter for the $7a_g$ orbital displays a rapid rise near threshold, followed by some weaker variations. For the $5b_u$ orbital (mainly σ-type O 2*p* lone-pair), the calculated $\beta$-parameter is somewhat similar to that predicted for the atomic O 2*p* orbital [19]. The theoretical results for the $1a_u$ and $1b_g$ orbitals (C=O π character) exhibit a characteristic energy dependence, namely a rapid rise from a low $\beta$-value at threshold to reach a high plateau value ($\beta$~1.5) above $h\nu$ ~50 eV, typical of that frequently observed and calculated [13-17,22,38] for a molecular π-type orbital.

Turning now to our experimental results, Fig. 5 shows an example of the $\theta = 0^o$ (parallel) and $\theta = 90^o$ (perpendicular) spectra recorded at a photon energy of 24.5 eV. Using Eqs (2) and (3), experimental mean photoelectron anisotropy parameters ($\beta$) and magic angle spectra can be extracted as a function of binding energy, and Fig. 6 displays the results so obtained at a photon energy of 41 eV. At this excitation energy, the Cooper minimum associated with the Cl 3*p* orbital leads, in the atomic case, to a $\beta$-value approaching zero [19]. In the binding energy range ~12.0 – 13.4 eV, the $\beta$-parameter for oxalyl chloride exhibits local minima at 12.25 and 12.85 eV, and local maxima at 12.61 and 13.10 eV. The values of the $\beta$-parameter at 12.25 and 12.61 eV are ~0.38 and 0.80, respectively, in reasonable accord with those calculated for the $6a_g$ and $2a_u$ orbitals (Fig. 4). Thus, the experimental photoelectron anisotropy measurements suggest that the binding energy of the $6a_g$ orbital is less than that of the $2a_u$ orbital, as predicted by those calculation methods (OVGF, EOM-IP-CCSD, TD-DFT) that include some treatment of electron correlation (Table 2).

The experimental evidence for the ordering of the next two orbitals, $2b_g$ and $6b_u$, is less conclusive. The local minimum in the $\beta$-value at a binding energy of ~12.85 eV, followed by the local maximum around 13.10 eV, suggests that the binding energy of the $6b_u$ orbital (essentially a σ-type Cl 3*p* lone-pair) is less than that of the $2b_g$ orbital. However, the value of the $\beta$-parameter in the minimum at 12.85 eV is ~0.71. This is much higher than the value (~0.0) predicted by our calculations for the $6b_u$ orbital (Fig. 4), and is also much higher than that predicted for atomic Cl 3*p* [19]. For the $2b_g$ orbital, our calculated $\beta$-value of ~0.65, at a photon energy of 41 eV, is in reasonable accord with the experimental value (0.79) at a binding energy of 13.10 eV. Hence, although the experimental $\beta$-parameters suggest that the binding energy of the $6b_u$ orbital is less than that of the $2b_g$ orbital, the measured value of the anisotropy parameter in the binding energy region where the contribution from the $6b_u$ orbital might be expected, is far higher than anticipated for a Cl 3*p* orbital.

To higher binding energy, the next orbital ($5b_u$) may be characterised as a strongly, though not uniquely, σ-type O 2*p* lone-pair (Fig. 1). Within the single particle model of ionization [37], ionization from such a non-bonding, localised molecular orbital might be expected to produce minimal vibrational excitation, so to appear as a single band in the photoelectron spectrum. In contrast to this expectation, in the anticipated $5b_u$ orbital region of the photoelectron spectrum of oxalyl chloride (Figs. 2, 5 and 6), our spectrum exhibits a doublet, with maxima at binding energies of ~13.39 and 13.61 eV. The measured $\beta$-parameters in the two maxima are not identical, and this disparity generally holds at other photon energies. The experimental value of the $\beta$-parameter at a photon energy of 41 eV is much lower than that (~1.3) predicted for atomic O 2*p* [19].

The current EOM calculations hint at a possible coupling of the $6B_u$ and $5B_u$ cation states, as both have significant transition amplitudes from the same pair of $6b_u$ and $5b_u$ orbitals, with amplitudes of 0.87 ($6b_u^{-1}$) and -0.42($5b_u^{-1}$) for the $6B_u$ state. For the $5B_u$ state these amplitudes effectively reverse to 0.43 ($6b_u^{-1}$) and 0.85 ($5b_u^{-1}$). The TD-DFT results likewise indicate very similar orbital transition amplitudes for these two states. Hence, these $B_u$ symmetry cation states appear to have some common heritage, despite both EOM and TD-DFT calculations

predicting a 0.3 eV energetic separation. While future theoretical studies will be required to investigate possible coupling in a detailed manner, it seems plausible that such a coupling may account for the absence of a low $\beta$-value in the binding energy region encompassing the contribution from the $6b_u$ orbital, the appearance of a doublet in the binding energy range ~13.4 – 13.6 eV, and the measured low value of the $\beta$-parameter in this doublet compared to the value expected for an O 2*p* orbital. In fact, the doublet structure tentatively associated with the $5b_u$ orbital is somewhat similar to that observed and treated theoretically for the $\tilde{B}\,^2A_1$ state in *cis*-dichloroethene [17,39].

Experimental state-selected photoelectron anisotropy parameters ($\beta$) have been extracted from the polarization dependent photoelectron spectra by averaging across each region listed in Table 1 (and also marked in Fig. 5). These are plotted as a function of photon energy in Fig. 4, where they may be compared with the theoretical curves. In general, a satisfactory qualitative agreement is found between the measured and calculated $\beta$-parameters, apart from that corresponding to binding energy region 5. The calculated $\beta$-parameter for this region, associated with the $6b_u$ orbital, exhibits a pronounced Cooper minimum that is not present in the experimental data. The effect of the Cl 3*p* Cooper minimum is, however, clearly evident in the $\beta$-parameter for the $6a_g$ orbital and, to a lesser extent, those for the $2a_u$ and $2b_g$ orbitals. This observation appears to support the suggestion of a coupling between the $6B_u$ and $5B_u$ cation states.

The experimental $\beta$-parameter recorded for the $1b_g$ ionization (region 7) calls for additional comment. As may be seen from Fig. 6, there is a very noticeable decrease in the $\beta$-value across the vibrational envelope of this band (from 1.2 to 0.6 in this particular example). This is contrary to expectations derived from the Franck-Condon approximation in which electronic and nuclear motions (vibrations) are fully decoupled — as for example appears in the flat $\beta$-parameter recorded across the vibrational envelope of the $7a_g^{-1}$ band in Fig. 6

In a given photoelectron band, the electron energy decreases across the vibrational envelope as the fixed photon energy is increasingly partitioned into vibrational excitation.

Conceivably, a variation in $\beta$ is just an energetic variation in the photoelectron scattering. This effect has been previously observed in the $\tilde{A}$ state spectrum of *cis*-dichloroethene recorded at a photon energy of 31 eV [17], where the incipient rapid decrease in $\beta$ on the low energy side of the Cl Cooper minimum produces a consequential weak rise (from 0.85 to 0.95) in the observed $\beta$ with increasing vibrational level (decreasing electron kinetic energy) across the band. In the present case, there is no evidence of a Cooper minimum in the $1b_g^{-1}$ ionization, and the much more marked variations in the $1b_g^{-1}$ $\beta$-parameter consistently appear as a *decrease* to high ionization energy at all photon energies studied here; there is no suggestion of a switch in the observed gradient as might be expected for alternate observations made to high and low photon energy sides of a putative Cl- Cooper minimum. Hence we discount this explanation.

We pursue this discussion with Fig. 7 which shows an expanded plot of $\beta$ across the $1b_g^{-1}$ state band recorded at a photon energy of 33 eV. The energy dependent variation in $\beta$ is similar to that in Fig. 6. Again, $\beta$ falls from 1.1 to 0.4 across the band to 16.2 eV, before rising through a maximum at ~16.6 eV. We can attribute this maximum to the $1a_u$ ionization (region 8). Viewed on this scale, the $\beta$-parameter displays clear vibrational structure. Superimposed on the overall trend of decrease with increasing excitation of the $\nu_1^+$ mode, there is a secondary trend for even more rapid decrease with the combinations involving quanta of the $\nu_5^+$ and $\nu_2^+$ modes. As stated, this is a clear violation of Franck-Condon based expectations. Despite the very regular, readily assigned appearance of this photoelectron band, we infer that this must evidence some vibronic interaction. Somewhat similar behaviour was noted in the $\tilde{D}$ band region of the *cis*-dichloroethene photoelectron spectrum [17] and a subsequent theoretical investigation identified the exact nature of the responsible $\tilde{D}/\tilde{E}$ state interaction [39].

Finally, it can be seen in Fig. 7 that the $\beta$-parameter curve shows a distinct peak appearing to the low energy side of the assigned $0^0$ origin. This behaviour is reproduced at other photon energies, and we tentatively attribute this to a $5_1^0$ vibrational hot band excitation. Although appearing far less distinct in the photoelectron spectrum, the hot band may perhaps be

discerned at the foot of the spectrum near 14.7 eV. Similar behaviour, with a thermal hot band excitation distinguished by different anisotropy, has again been noted in the $\tilde{D}$ band spectrum of *cis*-dichloroethene [17].

The theoretical photoionization partial cross sections for eight highest occupied orbitals in the ground state neutral molecule, obtained in our CMS-Xα calculations, are plotted in Fig. S3 of Supplementary material. These cross sections have been used to derive the theoretical branching ratios associated with the binding energy regions listed in Table 1. A comparison between the experimental and theoretical results (Fig. 8) shows a good overall agreement between the measured and calculated values. For the $5b_u$ orbital (region 6), the experimental branching ratio is significantly lower than predicted. This disparity suggests that either the binding energy range (13.30 – 14.20 eV) used for this region should be extended to lower energies, or that the theoretical partial cross section for the $5b_u$ orbital might be over-estimated. (It should be borne in mind, however, that since the branching ratios are normalized to unity, an over or under estimation in the ratio for one specific orbital affects the ratios for the remaining orbitals.)

The theoretical branching ratios for the $6a_g$, $2a_u$, $2b_g$ and $6b_u$ orbitals all display a reduction, at a photon energy around 40 eV, due to the Cl 3*p* Cooper minimum. Corresponding reductions are observed in the experimental results for the $6a_g$, $2a_u$ and $2b_g$ orbitals. Thus, the branching ratios for regions 2, 3 and 4 where the encompassed photoelectron bands are associated with orbitals possessing a strong Cl 3*p* character, provide evidence of the Cooper minimum affecting the photoionization dynamics. The apparent lack of a distinct minimum in the branching ratio for region 5 appears consistent with the results for the corresponding $\beta$-parameter (Fig. 4), namely that the photoelectron band occurring in region 5 should not be attributed simply to ionization of the $6b_u$ orbital.

## 5. Summary

The outer valence shell photoelectron spectrum of oxalyl chloride has been investigated experimentally by using plane polarized synchrotron radiation to record polarization

dependent spectra over the photon energy range 19 – 91 eV. These spectra have allowed photoelectron anisotropy parameters and branching ratios to be determined. In addition, a photoelectron spectrum of the complete valence shell has been recorded. This displays several broad bands, attributed to numerous satellite states whose intensity derives from electron correlation, in the inner valence region. The broad bands indicate that the single particle model of ionization [37], where ionization from a particular orbital gives rise to a single band in a photoelectron spectrum, is invalid. Under such circumstances, electron correlation redistributes the intensity associated with a specific inner valence orbital over many satellites of low intensity. The clustering of such states may result in broad peaks in the photoelectron spectrum.

The photoelectron spectrum of oxalyl chloride has also been studied theoretically by employing various levels of theory to calculate the orbital binding energies, and by using the CMS-Xα method to calculate photoionization partial cross sections and photoelectron angular distributions. The vertical ionization energies obtained in calculations employing methods which take electron correlation into account predict an energetic ordering of $6a_g$, $2a_u$, $2b_g$ and $6b_u$ for this group of closely spaced orbitals. All four of these orbitals possess a significant Cl 3*p* character.

The calculated photoelectron anisotropy parameters for the $6a_g$ and $6b_u$ orbitals, essentially σ-type Cl 3*p* lone-pairs, exhibit a pronounced minimum at a photon energy around 40 eV due to the atomic-like Cooper minimum. The calculated $\beta$-parameters for the $2a_u$ and $2b_g$ orbitals also exhibit a minimum, although less pronounced, around 40 eV. The measured $\beta$-values for the $6a_g$ orbital, and, to a lesser extent, those for the $2a_u$ and $2b_g$ orbitals are consistent with the theoretical predictions. However, the experimental anisotropy parameter associated with the $6b_u$ orbital shows little evidence of the predicted minimum around 40 eV.

In the region of the photoelectron spectrum where a band due to the $5b_u$ orbital might be expected, the experimental spectrum reveals a doublet. Our EOM calculations suggest a possible coupling of the $6B_u$ and $5B_u$ cation states. Such a coupling could provide a plausible

explanation for the unexpected appearance of the band nominally associated with the $5b_u$ orbital, for the discrepancy between the measured and calculated $\beta$-parameter associated with the $6b_u$ orbital in the photon energy range around 40 eV, and for the discrepancy between the measured and calculated $5b_u$ branching ratio.

The $1b_g$ photoelectron band displays vibrational structure which we are able to assign in terms of known vibrational modes from the neutral molecule. These form combinations involving $\nu_2^+$ and $\nu_5^+$, building upon a progression in $\nu_1^+$. Despite the apparent regularity and unexceptional intensity profile of this photoelectron band, the energy dependent variations in the $\beta$-parameter constitute a very strong departure from the Franck-Condon model of fully decoupled electron and nuclear motions, and so hint that vibronic interactions may play a significant role in this region of the spectrum.

**Acknowledgements**

DMPH is grateful to the Science and Technology Facilities Council (United Kingdom) for financial support. We are grateful for access to the University of Nottingham High Performance Computing Facility. We acknowledge the provision of beamtime by Synchrotron Soleil (beamtime Proposal No. 20150589), and we thank the technical staff at Soleil for their support and for the smooth operation of the facility.

Raw data were generated at the Synchrotron Soleil large scale facility. Derived data supporting the findings of this study are available from the corresponding author upon reasonable request.

**References**

[1] K. Hagen, K. Hedberg, J. Am. Chem. Soc. 95 (1973) 1003.

[2] D. D. Danielson, L. Hedberg, K. Hedberg, K. Hagen, M. Trætteberg, J. Phys. Chem. 99 (1995) 9374.

[3] J. R. Durig, J. F. Davis, A. Wang, J. Mol. Struct. 375 (1996) 67.

[4] M. L. Senent, J. Mol. Struct. 406 (1997) 51.

[5] S. –H. Chien, K. –C. Lau, W. –K. Li, C. Y. Ng, J. Phys. Chem. A 103 (1999) 7918.

[6] G. Chu, J. Chen, F. Liu, X. Shan, J. Han, L. Sheng, Chem. Phys. 416 (2013) 26.

[7] D. C. Frost, C. A. McDowell, G. Pouzard, N. P. C. Westwood, J. Electron Spectrosc. Relat. Phenom. 10 (1977) 273.

[8] K. Kimura, S. Katsumata, Y. Achiba, T. Yamazaki, S. Iwata, Handbook of HeI Photoelectron Spectra of Fundamental Organic Molecules, Japan Scientific Societies Press, Tokyo, 1981.

[9] C. –Y. Wu, Y. –P. Lee, N. S. Wang, J. Chem. Phys. 120 (2004) 6957.

[10] M. Ahmed, D. Blunt, D. Chen, A. G. Suits, J. Chem. Phys. 106 (1997) 7617.

[11] R. S. Mulliken, J. Chem. Phys. 23 (1955) 1833.

[12] D. M. P. Holland, I. Powis, G. Öhrwall, L. Karlsson, W. von Niessen, Chem. Phys. 326 (2006) 535.

[13] A. W. Potts, D. M. P. Holland, I. Powis, L. Karlsson, A. B. Trofimov, I. L. Dodzuk, Chem. Phys. 415 (2013) 84.

[14] I. Powis, A. B. Trofimov, I. L. Bodzuk, D. M. P. Holland. A. W. Potts, L. Karlsson, Chem. Phys. 415 (2013) 291.

[15] D. M. P. Holland, I. Powis, A. B. Trofimov, I. L. Bodzuk, D. Yu. Sosnikov, A. W. Potts, L. Karlsson, Chem. Phys. 448 (2015) 61.

[16] D. M. P. Holland, I. Powis, A. B. Trofimov, R. C. Menzies, A. W. Potts, L. Karlsson, I. L. Badsyuk, T. E. Moskovskaya, E. V. Gromov, J. Schirmer, J. Chem. Phys. 147 (2017) 164307.

[17] I. Powis, R. C. Menzies, D. M. P. Holland, A. B. Trofimov, A. D. Skitnevskaya, E. V. Gromov, E. Antonsson, M. Patanen, C. Nicolas, C. Miron, J. Chem. Phys. 149 (2018) 074305.

[18] Y. Hikosaka, J. H. D. Eland, T. M. Watson, I. Powis, J. Chem. Phys. 115 (2001) 4593.

[19] S. T. Manson, A. Msezane, A. F. Starace, S. Shahabi, Phys. Rev. A 20 (1979) 1005.

[20] J. W. Cooper, Phys. Rev. 128 (1962) 681.

[21] U. Fano and J. W. Cooper, Rev. Mod. Phys. 40 (1968) 441.

[22] I. Powis, D. M. P. Holland, E. Antonsson, M. Patanen, C. Nicolas, C. Miron, M. Schneider, D. Yu. Soshnikov, A. Dreuw, A. B. Trofimov, J. Chem. Phys. 143 (2015) 144304.

[23] R. Forbes, S. T. Pratt, A. De Fanis, A. R. Milosavljević, C. Nicolas, J. D. Bozek, N. A. Besley, D. M. P. Holland, Phys. Rev. A 101 (2020) 023408.

[24] P. Baltzer, L. Karlsson, M. Lundqvist, B. Wannberg, Rev. Sci. Instrum. 64 (1993) 2179.

[25] C. N. Yang, Phys. Rev. 74 (1948) 764.

[26] J. Jauhiainen, A. Ausmees, A. Kivimäki, S. J. Osborne, A. Naves de Brito, S. Aksela, S. Svensson, H. Aksela, J. Electron Spectrosc. Relat. Phenom. 69 (1994) 181.

[27] B. Wannberg, D. Nordfors, K. L. Tan, L. Karlsson, L. Mattsson, J. Electron Spectrosc. Relat. Phenom. 47 (1988) 147.

[28] P. Baltzer, F. T. Chau, J. H. D. Eland, L. Karlsson, M. Lundqvist, J. Rostas, K. Y. Tam, H. Veenhuizen, B. Wannberg, J. Chem. Phys. 104 (1996) 8922.

[29] J. Liu, M. Hochlaf, C. Y. Ng, J. Chem. Phys. 113 (2000) 7988.

[30] M. J. Frisch et al, Gaussian 16, Revision A.03. Gaussian Inc., Wallingford, CT, 2016.

[31] V. G. Zakrzewski, J. V. Ortiz, J. A. Nichols, D. Heryadi, D. L. Yeager, J. T. Golab, Int. J. Quantum Chem. 60 (1996) 29.

[32] V. G. Zakrzewski, O. Dolgounitcheva, J. V. Ortiz, J. Chem. Phys. 105 (1996) 8748.

[33] Y. Shao et al, Mol. Phys. 113 (2015) 184.

[34] J. F. Stanton, J. Gauss, J. Chem. Phys. 101 (1994) 8938.

[35] A. I. Krylov, Annu. Rev. Phys. Chem. 59 (2008) 433.

[36] D. Edvardsson, P. Baltzer, L. Karlsson, M. Lundqvist, B. Wannberg, J. Electron Spectrosc. Relat. Phenom. 73 (1995) 105.

[37] L. S. Cederbaum, W. Domcke, J. Schirmer, W. von Niessen, Adv. Chem. Phys. 65, (1986) 115.

[38] D. M. P. Holland, L. Karlsson, W. von Niessen, J. Electron Spectrosc. Relat. Phenom. 113 (2001) 221.

[39] A. B. Trofimov, I. Powis, R. C. Menzies, D. M. P. Holland, E. Antonsson, M. Patanen, C. Nicolas, C. Miron, A. D. Skitnevskaya, E. V. Gromov, H. Köppel, J. Chem. Phys. 149 (2018) 074306.

Table 1

Binding energy regions used to evaluate the photoelectron anisotropy parameters and branching ratios of oxalyl chloride

| Region | Binding energy range (eV) | Encompassed orbitals |
|---|---|---|
| 1 | 10.70 – 11.85 | $7a_g$ |
| 2 | 12.00 – 12.45 | $6a_g$ |
| 3 | 12.45 – 12.77 | $2a_u$ |
| 4 | 12.77 – 12.98 | $2b_g$ |
| 5 | 12.98 – 13.30 | $6b_u$ |
| 6 | 13.30 – 14.20 | $5b_u$ |
| 7 | 14.60 – 16.45 | $1b_g$ |
| 8 | 16.45 – 17.60 | $1a_u$, ($5a_g$?)[a], ($4b_u$?)[a] |

[a] It is uncertain where the contribution from this orbital appears in the photoelectron spectrum

Table 2

Calculated vertical ionization energies in eV of the valence orbitals of oxalyl chloride (*trans* $C_{2h}$ geometry)

| Orbital | Koopmans[a] (eV) | OVGF [b] | | OVGF [c] | | EOM-CCSD [d] | | TD-DFT [e] |
|---|---|---|---|---|---|---|---|---|
| | | I.E. | Pole Strength | I.E. | Pole Strength | Aug-cc-pVTZ | cc-pVQZ | B3LYP/cc-pVQZ |
| $1a_g$ | 40.65 | | | | | | | |
| $1b_u$ | 40.18 | | | | | | | |
| $2a_g$ | 32.07 | | | | | | | |
| $2b_u$ | 31.95 | | | | | | | |
| $3a_g$ | 25.95 | | | | | | | |
| $3b_u$ | 21.29 | | | | | 19.01 | 19.07 | |
| $4a_g$ | 20.28 | 17.98 | 0.86 | 18.00 | 0.859 | 17.94 | 18.00 | |
| $4b_u$ | 19.67 | 17.69 | 0.867 | 17.73 | 0.867 | 17.58 | 17.65 | |
| $5a_g$ | 18.39 | 16.53 | 0.878 | 16.57 | 0.878 | 16.53 | 16.60 | |
| $1a_u$ | 18.08 | 16.82 | 0.869 | 16.84 | 0.869 | 17.05 | 17.10 | |
| $1b_g$ | 16.28 | 15.21 | 0.872 | 15.22 | 0.872 | 15.35 | 15.40 | 15.03 |
| $5b_u$ | 15.29 | 13.56 | 0.879 | 13.56 | 0.879 | 13.39 | 13.46 | 13.38 |
| $6b_u$ | 13.99 | 13.04 | 0.9 | 13.09 | 0.9 | 13.07 | 13.14 | 12.90 |
| $2b_g$ | 13.69 | 12.87 | 0.898 | 12.92 | 0.898 | 13.00 | 13.07 | 12.70 |
| $2a_u$ | 13.38 | 12.59 | 0.898 | 12.63 | 0.898 | 12.71 | 12.78 | 12.46 |
| $6a_g$ | 13.35 | 12.37 | 0.903 | 12.41 | 0.903 | 12.52 | 12.59 | 12.33 |
| $7a_g$ | 12.80 | 11.46 | 0.894 | 11.45 | 0.894 | 11.35 | 11.42 | (11.4) |

[a] MP2/cc-pVQZ

[b] OVGF/aug-cc-pVTZ//MP2/cc-pVTZ

[c] OVGF/cc-pVQZ//MP2/cc-pVQZ

[d] EOM-IP-CCSD with indicated basis sets at the MP2/cc-pVTZ optimised geometry.

[e] TD-DFT calculation (B3LYP/cc-pVQZ) of excited cation states but performed at the MP2/cc-pVTZ *neutral* equilibrium geometry. Ionization energy estimates obtained by adding an assumed $I_{vert}$ = 11.4eV for the $7a_g^{-1}$ ground state to the electronic excitation energies.

Table 3

Excitation energies and proposed assignments for the vibrational structure observed in the photoelectron band associated with the $1b_g$ orbital

| Vibrational assignment | Excitation energy (eV) |
|---|---|
| $0^0$ | 14.774 |
| $1^1$ | 15.004 |
| $1^2$ | 15.232 |
| $1^3$ | 15.458 |
| $1^4$ | 15.684 |
| $1^5$ | 15.918 |
| $5^1$ | 14.814 |
| $1^1 5^1$ | 15.044 |
| $1^2 5^1$ | 15.270 |
| $1^3 5^1$ | 15.492 |
| $5^2$ | 14.858 |
| $1^1 5^2$ | 15.084 |
| $2^1$ | 14.914 |
| $1^1 2^1$ | 15.144 |

Figure Captions

Figure 1. Iso-surface plots of the eight highest occupied orbitals in the neutral ground state of oxalyl chloride. The green and red sticks correspond to the chlorine and oxygen atoms, respectively.

Figure 2. The magic angle photoelectron spectrum of oxalyl chloride obtained at a photon energy of 19 eV. Vertical ionization energies obtained by EOM-IP-CCSD/aug-cc-pVTZ calculations are marked by vertical arrows: filled arrow heads indicate results for the dominant *trans* conformer (Table 2); open arrow heads indicate results for the minor *gauche* conformer. The extended valence shell photoelectron spectrum of oxalyl chloride, recorded at a photon energy of 80 eV using parallel polarized synchrotron radiation, is included as an inset to this figure.

Figure 3. The photoelectron band due to ionization of the $1b_g$ orbital, recorded at a photon energy of 23 eV using parallel polarized synchrotron radiation. The vibrational structure can be assigned to four progressions, each involving excitation of the $\nu_1^+$ mode, either alone, or in combination with one or two quanta of the $\nu_5^+$ mode, or one quantum of the $\nu_2^+$ mode. Excitation energies are given in Table 3.

Figure 4. Photoelectron anisotropy parameters ($\beta$) for the outer valence orbitals of oxalyl chloride. The theoretical result for each orbital, calculated with the CMS-Xα method, is plotted as a red continuous line. The corresponding experimental result, associated with a specific binding energy region (Table 1), is plotted as a blue dot, with each dot being joined by a straight line. The error bars representing the statistical uncertainty only, are smaller than the plotting symbol.

Figure 5. Photoelectron spectra of oxalyl chloride, obtained at a photon energy of 24.5 eV, recorded with plane polarized radiation with the plane of polarization set parallel ($\theta$ = 0°) or perpendicular ($\theta$ = 90°) to the electron's path towards the detector. These raw spectra have not been corrected for the transmission efficiency of the electron spectrometer. The numbers close to the bottom of the figure denote the regions (Table 1), marked by vertical dotted lines, used to analyse the spectra.

Figure 6. The magic angle photoelectron spectrum (blue) of oxalyl chloride obtained at a photon energy of 41 eV and the corresponding photoelectron anisotropy parameter (red). Also shown are calculated EOM-IP-CCSD/Aug-cc-pVTZ vertical ionization energies. The photoelectron spectrum is arbitrarily scaled.

Figure 7. Expanded view of the $(1b_g)^{-1}$ state band (region 7) recorded at $h\nu$ = 33 eV showing the photoelectron spectrum with arbitrary scaling, and the $\beta$-parameter.

Figure 8. The photoelectron branching ratios for the outer valence orbitals of oxalyl chloride. The theoretical result for each orbital, obtained from the photoionization cross sections calculated with the CMS-Xα method, is plotted as a red continuous line. The corresponding experimental result, associated with a specific binding energy region (Table 1), is plotted as a blue dot, with each dot being joined by a straight line. The error bars representing the statistical uncertainty only, are smaller than the plotting symbol.

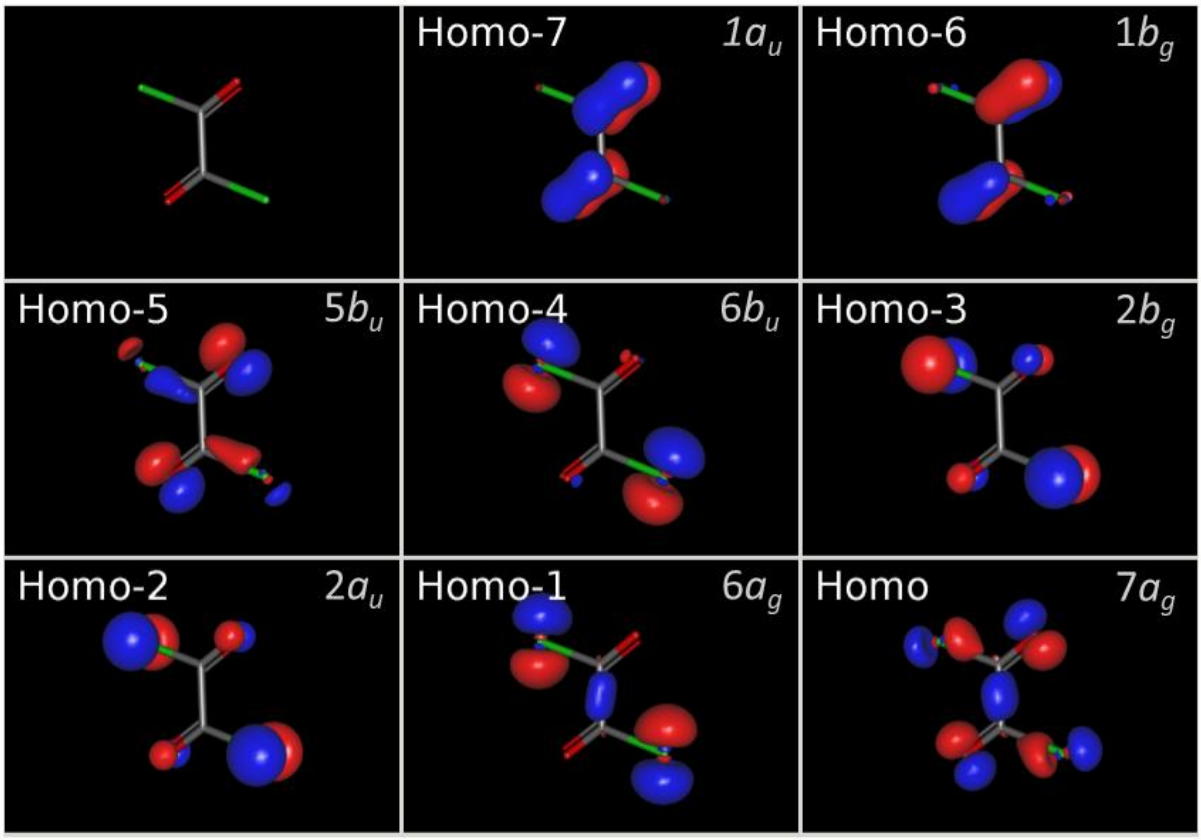
Homo-7
$1a_u$
Homo-6
$1b_g$
Homo-5
$5b_u$
Homo-4
$6b_u$
Homo-3
$2b_g$
Homo-2
$2a_u$
Homo-1
$6a_g$
Homo
$7a_g$

Figure 1

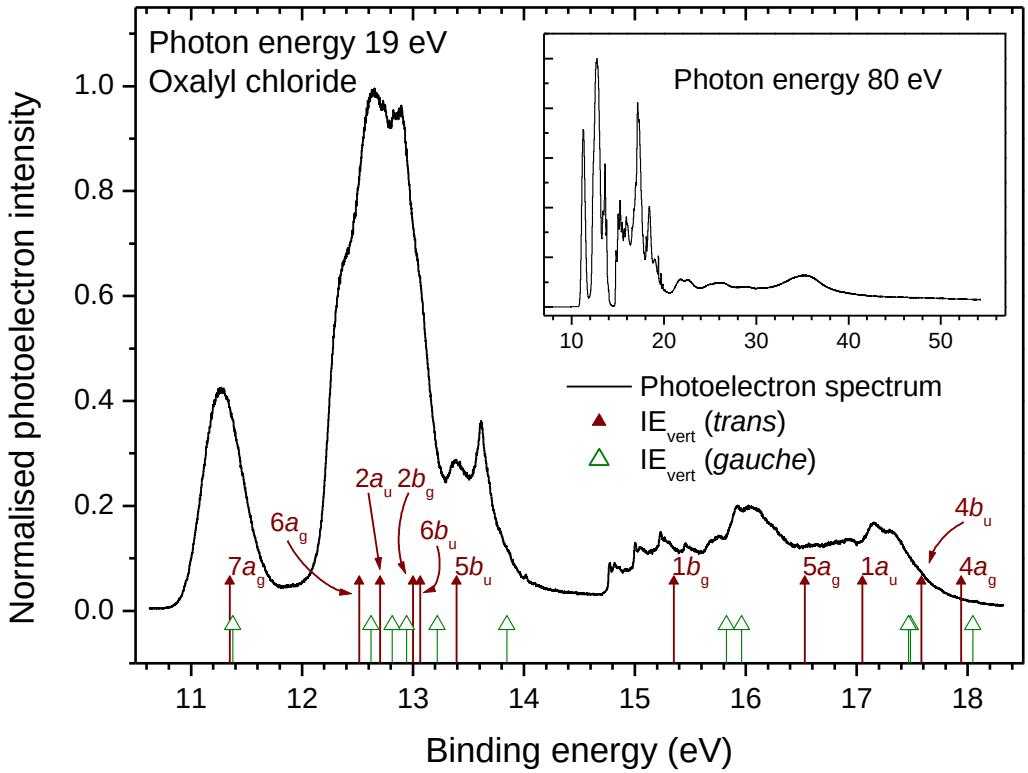
Photon energy 19 eV
Oxalyl chloride
Photon energy 80 eV
Photoelectron spectrum
IE$_{vert}$ (*trans*)
IE$_{vert}$ (*gauche*)
Normalised photoelectron intensity
Binding energy (eV)
7a$_g$
6a$_g$
2a$_u$
2b$_g$
6b$_u$
5b$_u$
1b$_g$
5a$_g$
1a$_u$
4b$_u$
4a$_g$

Figure 2

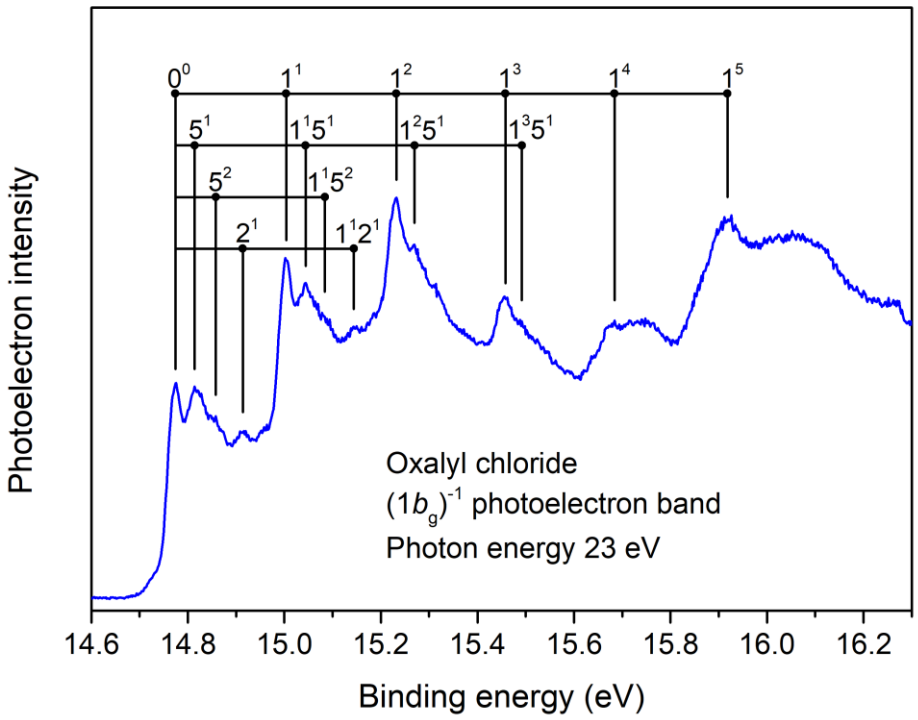
$0^0$
$1^1$
$1^2$
$1^3$
$1^4$
$1^5$
$5^1$
$1^15^1$
$1^25^1$
$1^35^1$
$5^2$
$1^15^2$
$2^1$
$1^12^1$
Oxalyl chloride
$(1b_g)^{-1}$ photoelectron band
Photon energy 23 eV
Photoelectron intensity
14.6
14.8
15.0
15.2
15.4
15.6
15.8
16.0
16.2
Binding energy (eV)

Figure 3

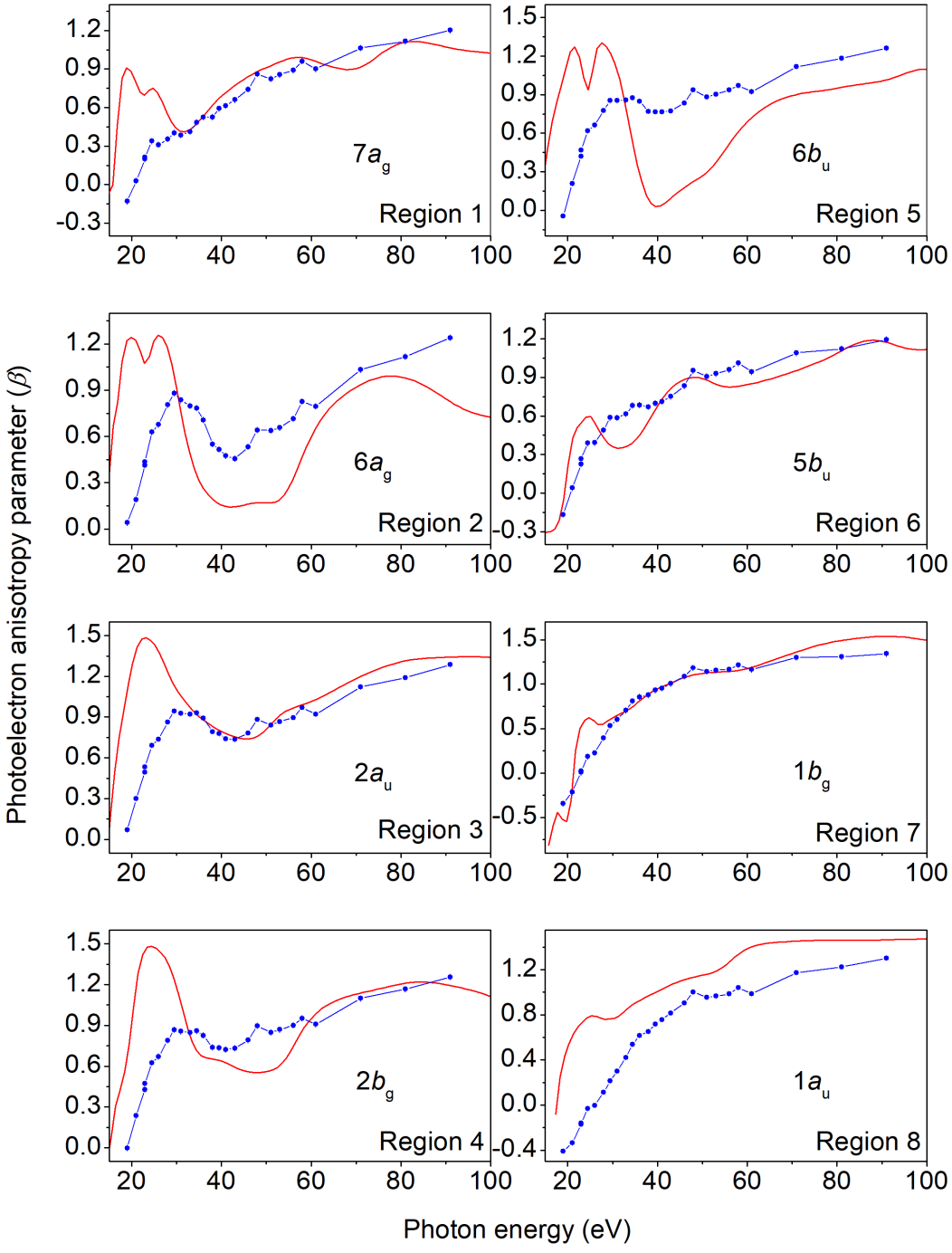
Photoelectron anisotropy parameter (β)
Photon energy (eV)
7a_g
Region 1
6b_u
Region 5
6a_g
Region 2
5b_u
Region 6
2a_u
Region 3
1b_g
Region 7
2b_g
Region 4
1a_u
Region 8

Figure 4

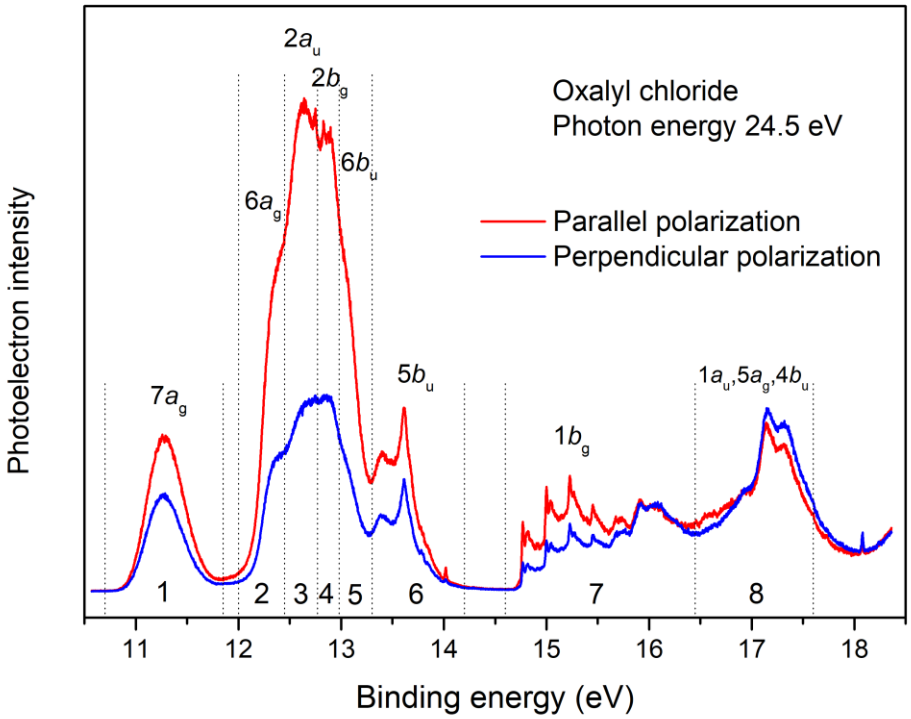
Oxalyl chloride
Photon energy 24.5 eV
Parallel polarization
Perpendicular polarization
Photoelectron intensity
Binding energy (eV)
2a_u
2b_g
6b_u
6a_g
7a_g
5b_u
1b_g
1a_u,5a_g,4b_u
1
2
3
4
5
6
7
8
11
12
13
14
15
16
17
18

Figure 5

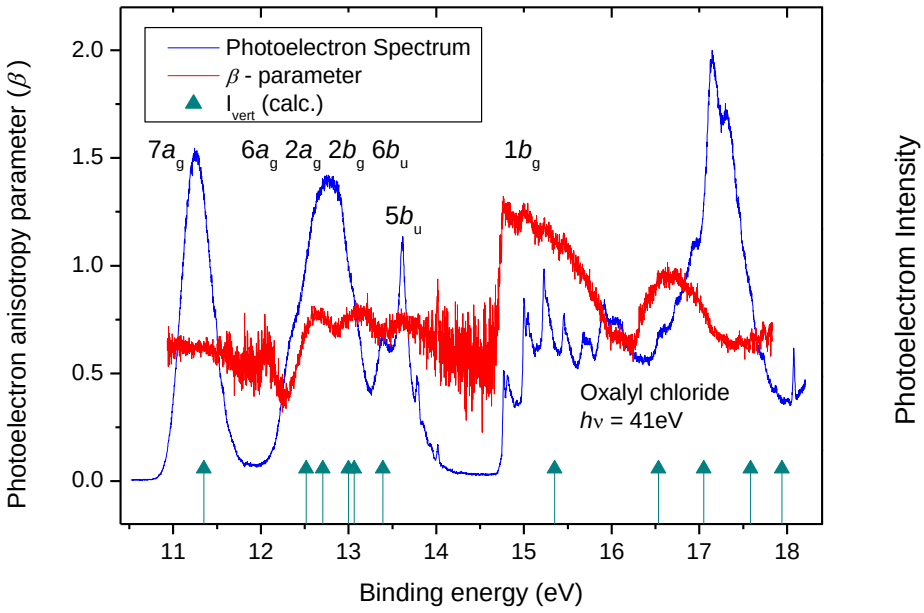
Photoelectron Spectrum
β - parameter
I vert (calc.)
7a g
6a g 2a g 2b g 6b u
5b u
1b g
Oxalyl chloride
hν = 41eV
Photoelectron anisotropy parameter (β)
Photoelectrom Intensity
Binding energy (eV)
2.0
1.5
1.0
0.5
0.0
11
12
13
14
15
16
17
18

Figure 6

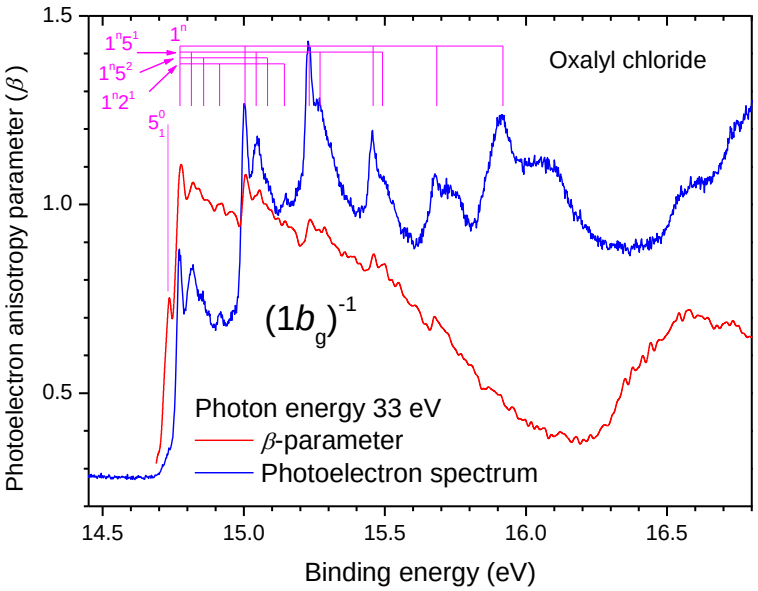
Photoelectron anisotropy parameter ($\beta$)
1.5
1.0
0.5
14.5
15.0
15.5
16.0
16.5
Binding energy (eV)
$1^n5^1$
$1^n$
$1^n5^2$
$1^n2^1$
$5^0_1$
Oxalyl chloride
$(1b_g)^{-1}$
Photon energy 33 eV
$\beta$-parameter
Photoelectron spectrum

Figure 7

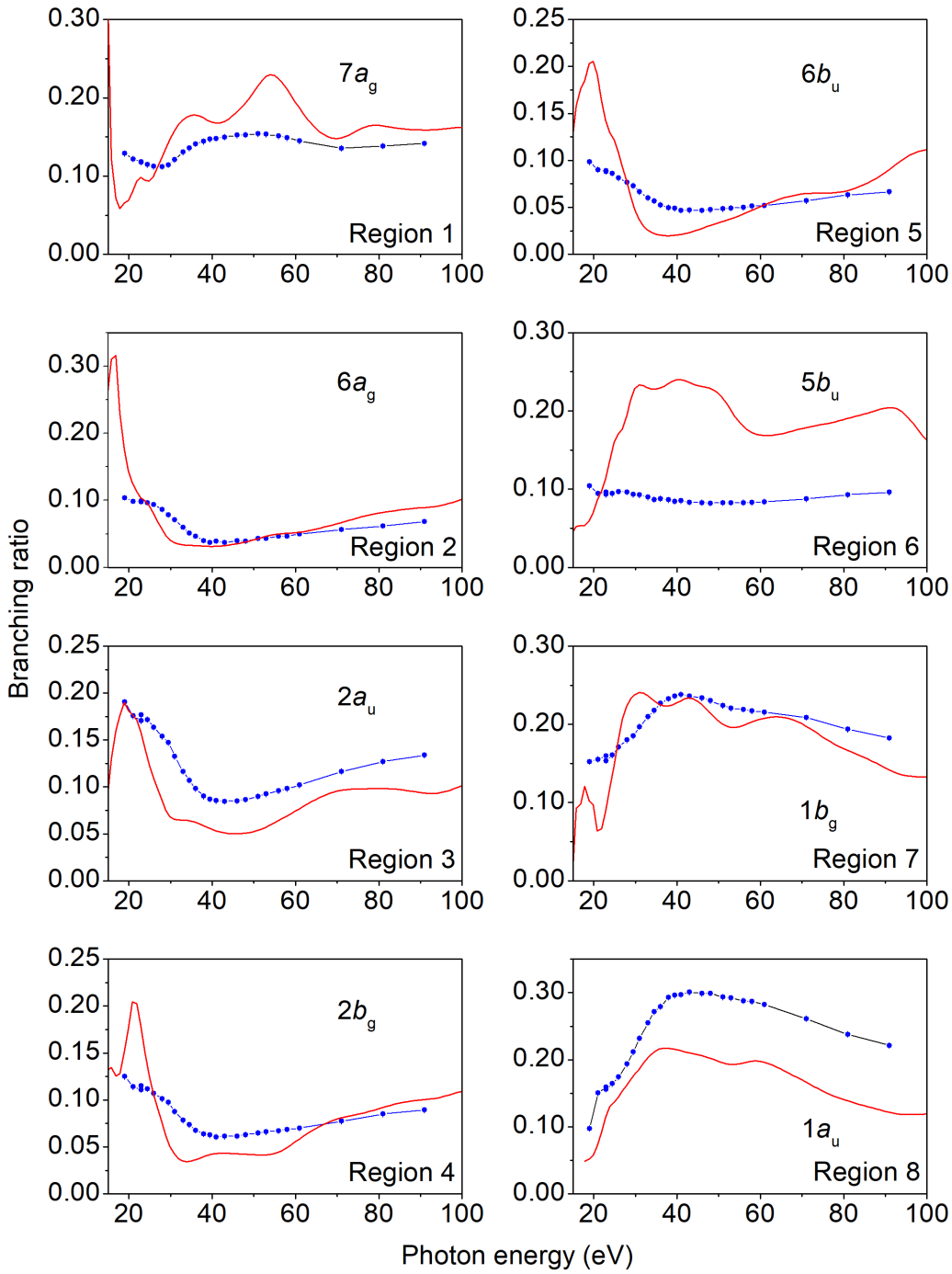
Branching ratio
Photon energy (eV)
7$a_g$
Region 1
6$b_u$
Region 5
6$a_g$
Region 2
5$b_u$
Region 6
2$a_u$
Region 3
1$b_g$
Region 7
2$b_g$
Region 4
1$a_u$
Region 8

Figure 8